Characterization of Self-Assembled Lamellar Thermoresponsive Silica−Hydrogel Nanocomposite Films

G. Garnweitner,[†,‡] B. Smarsly,*[,†,‡] R. Assink,[§] D. R. Dunphy,[§] C. Scullin,[‡] and C. J. Brinker[‡,§]

Max Planck Institute of Colloids and Interfaces, Am Mühlenberg 1, D-14476 Potsdam-Golm, Germany, University of New Mexico, Advanced Materials Lab, 1001 University Boulevard, Albuquerque, New Mexico 87106, and Sandia National Laboratories, MS 1349, Albuquerque, New Mexico 87185

Received April 26, 2004. In Final Form: July 8, 2004

Mesostructured lamellar nanocomposite films with alternating silica and organic layers containing poly(*N*-isopropropyl acrylamide) (PNIPAM) were prepared using evaporation-induced self-assembly. A suitable theoretical approach to analyze the small-angle X-ray scattering (SAXS) patterns of oriented lamellar two-phase systems was applied to the SAXS data of films of varying composition, providing details on the self-assembly process, the composition, and the polymerization. In particular, this approach allowed an accurate determination of the thickness of the silica and the organic layer. The applicability of the SAXS approach was carefully tested with simulated data and verified by thermogravimetric analysis (TGA). TGA and ^{13}C NMR were used to study the polymerization and linkage to the silica matrix. SAXS and time-resolved grazing incidence SAXS revealed that the phase transition of PNIPAM at ca. 32 °C leads to a reversible expansion/contraction perpendicular to the layers on a time scale of ca. 30 min.

Introduction

The preparation of surfactant-templated inorganic/organic nanocomposite thin films possessing various types of ordered mesostructures such as 2D hexagonal or 3D cubic lattices has attained great attention because of straightforward coating preparation using evaporation-induced self-assembly (EISA).[1] In the EISA procedure, typically a substrate is dip-coated or spin-coated with an acidic aqueous solution of a structure-directing surfactant and a silica precursor such as TEOS (tetraethyl orthosilicate) in a water-miscible, volatile solvent (e.g., ethanol). The surfactant concentration increases upon evaporation of the solvent, and at a certain concentration co-self-assembly occurs, leading to structures such as lamellae, cylindrical rods, and so forth.[2] While so far EISA has been used mainly to generate ordered mesoporous films, the incorporation of functional organic moieties into mesostructured films would be of particular interest, especially with polymers as the organic part. The general underlying idea is to combine interesting optical,[3] electronic,[4−6] thermal,[7,8] and mechanical[9,10] properties of polymers with the features of an inorganic framework. For further information, see for example ref 11. While most of these studies focused on bulk materials, the number of publications on thin films is significantly smaller due to the difficulty in processing polymers and inorganics on the nanometer scale in thin films. One of the fundamental problems is to avoid a disturbance of the self-assembly by the presence of polymers. Also, it is difficult to achieve a homogeneous distribution of the polymers in the mesostructure throughout the entire film. The strategies for the preparation of polymer−inorganic self-assembled coatings can be classified into four general routes:

(1) A preformed porous film (obtained by EISA) is soaked with an organic monomer or the polymer itself.

(2) The monomer is covalently linked to the inorganic (siliceous) precursor.[9]

(3) Molecules are used acting as both structure-directing agents and monomers ("surfmers"). This method was used to prepare poly(diacetylene)/silica[3a] and silica/conductive polymer nanocomposite films.[12,13]

(4) Monomers are added to the precursor solution, thus being embedded between the inorganic walls during the self-assembly, and are polymerized in a subsequent

* To whom correspondence should be addressed. E-mail: smarsly@mpikg-golm.mpg.de.

† Max Planck Institute of Colloids and Interfaces.

‡ University of New Mexico.

§ Sandia National Laboratories.

(1) (a) Brinker, C. J.; Lu, Y. F.; Sellinger, A.; Fan H. Y. *Adv. Mater.* **1999**, *11*, 579−585. (b) Grosso, D.; Balkenende, A. R.; Albouy, P. A.; Lavergne, M.; Babonneau, F. *J. Mater. Chem.* **2000**, *10*, 2085−2089. (c) Grosso, D.; Babonneau, F.; Albouy, P. A.; Amenitsch, H.; Balkenende, A. R.; Brunet-Bruneau, A.; Rivory, J. *Chem. Mater.* **2002**, *2*, 931−939. (d) Besson, S.; Gacoin, T.; Jacquiot, C.; Ricolleau, C.; Babonneau, F.; Boilot, J.-P. *J. Mater. Chem.* **2000**, *10*, 1331−1337.

(2) (a) Grosso, D.; Balkenende, A. R.; Albouy, P. A.; Ayral, A.; Amenitsch, H.; Babonneau, F. *Chem. Mater.* **2001**, *13*, 1848−1856. (b) Grosso, D.; Babonneau, F.; Soler-Illia, G. J. A. A.; Albouy, P. A.; Amenitsch, H. *Chem. Commun.* **2002**, 748−749. (c) Klotz, M.; Albouy, P. A.; Ayral, A.; Ménager, C.; Grosso, D.; Van der Lee, A.; Cabuil, V.; Guizard, C. *Chem. Mater.* **2000**, *12*, 1721−1728. (d) Gibaud, A.; Grosso, D.; Smarsly, B.; Baptiste, A.; Bardeau, J. F.; Babonneau, F.; Doshi, D. A.; Chen, Z.; Brinker, C. J.; Sanchez, C. *J. Phys. Chem. B* **2003**, *107*, 6114−6118.

(3) (a) Yang, Y.; Lu, Y. F.; Lu, M. C.; Huang, J. M.; Haddad, R.; Xomeritakis, G.; Liu, N. G.; Malanoski, A. P.; Sturmayr, D.; Fan, H. Y.; Sasaki, D. Y.; Assink, R. A.; Shelnutt, J. A.; van Swol, F.; Lopez, G. P.; Burns, A. R.; Brinker, C. J. *J. Am. Chem. Soc.* **2003**, *125*, 1269−1277. (b) Lu, Y. F.; Yang, Y.; Sellinger, A.; Lu, M. C.; Huang, J. M.; Fan, H. Y.; Haddad, R.; Lopez, G.; Burns, A. R.; Sasaki, D. Y.; Shelnutt, J.; Brinker, C. J. *Nature* **2001**, *410*, 913−917.

(4) Lee, Y.; Kim, J.; Son, Y. *Polymer* (*Korea*) **1999**, *23*, 443−449.

(5) Wu, C. G.; Bein, T. *Stud. Surf. Sci. Catal.* **1994**, *84*, 2269−2276.

(6) Nguyen, T. Q.; Wu, J. J.; Doan, V.; Schwartz, B. J.; Tolbert, S. H. *Science* **2000**, *288*, 652−656.

(7) Liang, L.; Liu, J.; Gong, X. *Langmuir* **2000**, *16*, 9895−9899.

(8) Enzel, P.; Bein, T. *Chem. Mater.* **1992**, *4*, 819−824.

(9) Soppera, O.; Croutxe-Barghorn, C.; Carre, C.; Blanc, D. *Appl. Surf. Sci.* **2002**, *186*, 91−94.

(10) Sellinger, A.; Weiss, P. M.; Nguyen, A.; Lu, Y.; Assink, R. A.; Gong, W.; Brinker, C. J. *Nature* **1998**, 394, 256−260.

(11) Bein, T. *Stud. Surf. Sci. Catal.* **1996**, *102*, 295−322.

(12) Ikegame, M.; Tajima, K.; Aida, T. *Angew. Chem., Int. Ed.* **2003**, *42*, 2154−2157.

(13) Li, G. T.; Bhosale, S.; Wang, T. Y.; Zhang, Y.; Zhu, H. S.; Fuhrhop, K. H. *Angew. Chem., Int. Ed.* **2003**, *42*, 3818−3821.

10.1021/la048962x CCC: $27.50
Published on Web 09/23/2004

Chart 1. Chemical Structures of NIPAM (a), DM (b), and 7-OTS (c)

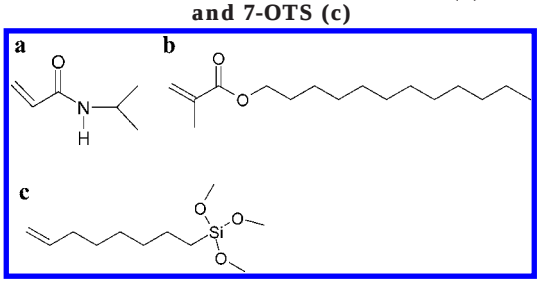

step.[10,14] The polymer can be connected covalently to the inorganic matrix through coupling agents (CAs) featuring an alkoxide group and a polymerizable double bond.

While route 1 is the most simple one in terms of processing, it suffers from a possible inhomogeneous distribution of the polymer in the mesoporous host due to diffusion problems. Routes 2 and 3 have the advantage of a high and well-defined monomer concentration inside the mesostructure; however, these approaches require the design of suitable monomers for each system. Although in route 4 the integration of the monomer content is more difficult to control, a variety of commercially available and cheap monomers and surfactants can be combined without further synthetic effort.

Using route 4, the present study is focused on the fabrication of lamellar nanocomposites of silica with hydrogels, which are polymers showing a pronounced uptake of water ("swelling") and also environmental responsiveness. In particular, poly(*N*-isopropropyl acrylamide) (PNIPAM) shows a phase transition at about 32 °C in water.[15] It has been previously shown that PNIPAM can be incorporated into a clay composite,[7,16] and recently we reported the incorporation of copolymers of NIPAM with dodecyl methacrylate (DM) into lamellar mesostructured nanocomposite silica films using EISA[14] (see Chart 1 for chemical structures). A coupling agent (trimethoxy(7-octen-1-yl)silane, 7-OTS) is added and supposed to link the polymer chains covalently to the silica matrix. In essence, we showed that the thermoresponsiveness was intact, leading to a reversible expansion of lamellar mesostructures. In short, the present study is aimed at a deeper understanding of the various parameters involved in route 4.

In particular, the fabrication of nanocomposite polymer/silica films requires a thorough characterization in terms of the successful polymer incorporation, mesostructural homogeneity, and composition. Obviously, compared to mesoporous thin films the characterization of polymer/inorganic nanocomposite films is more complex, because standard techniques such as physisorption cannot be used. In principle, small-angle X-ray scattering (SAXS) is nondestructive and an ideal method to characterize nanocomposite inorganic/organic films. Although the technique has been extensively applied to study lamellar nanocomposites such as clays, to the best of our knowledge no study aimed at a detailed quantitative evaluation of SAXS in symmetric reflection, in particular in terms of the thickness of the single layers d_1 and d_2 of the siliceous layer and the organic phase, respectively. Usually, the interpretation of such data does not go beyond the determination of the d spacing.[10,12,13] In our recent publication,[14a] a quantitative SAXS evaluation approach was successfully applied with respect to several structural parameters. In essence, this approach is based on fitting the entire SAXS curve with a limited number of physical parameters such as d_1 and d_2 and their variances σ_1 and σ_2, based on a two-phase model of alternating layers. While the theory is presented in detail in a separate publication,[17] here we address more practical aspects of this approach:

(i) The approach is tested with simulated SAXS data of lamellar mesostructures to verify the accuracy of the parameters d_1, d_2, σ_1, and σ_2 obtained from nonlinear fitting procedures.

(ii) The determination of the most important parameters d_1 (silica layers) and d_2 (organic layers) from SAXS is compared with data from thermogravimetric analysis (TGA), the latter providing the overall silica and organic content. d_1 and d_2 should correspond to the relative weight ratio determined from TGA, if the SAXS approach is reliable.

(iii) The SAXS method is applied to SAXS curves of various silica−organic nanocomposite films of different composition, for example, with and without polymer, and different treatments, that is, prior to and after the polymerization (see Table 2). This series was considered as a test for the general applicability of our approach but also as a method to reveal important information on the mesostructure and chemical composition.

In contrast to previous SAXS studies on similar materials, our approach takes exactly into account experimental features (smearing, absorption correction) and orientation effects.

In addition, the present work addresses further physicochemical aspects of the polymer/silica nanocomposite films (see sections 3−6). The polymerization of NIPAM with DM and the linkage to the silica matrix were studied by NMR and TGA with respect to the incorporation into the films and to the formation of random or more blocklike copolymers. Preliminary experiments had indicated that the addition of DM is needed to maintain a stable thermoresponsive film, but the details had remained unclear. We also provide evidence by TGA that the polymer is located not within the silica matrix but in separate organic layers. As important practical features, the water uptake/release behavior of hydrogel/silica nanocomposite films and their stability against water were investigated by spectroscopic ellipsometry. Finally, the swelling behavior and kinetics of the lamellar hydrogel nanocomposites are described in further detail by SAXS and, for the first time, also in situ 2D grazing incidence small-angle X-ray scattering (GISAXS) (section 6). Thereby, the SAXS methods presented in this study establish a new methodology for the characterization of functional polymer−inorganic nanocomposite thin films in general.

Experimental Section

The sample preparation is based on the procedure described in our recent publication. Typically, a homogeneous solution was prepared by mixing an acidic silica sol, monomers (NIPAM and/or dodecyl methacrylate), and surfactant (cetyltrimethylammonium bromide, CTAB) in ethanol. The coupling agent (7-OTS), featuring an alkoxysilane headgroup and a polymerizable double bond, was added along with the thermal initiator, 1,1′-azobis-(1-cyclohexanecarbonitrile) (ACHN) (initiators such as persulfates were incompatible with the procedure). The molar ratio of reactants was 1 TEOS/22 EtOH/5 H_2O/0.004 HCl/0.21 CTAB/0.16 7-OTS/0.32 DM/(0−0.14) NIPAAM/0.02 initiator. After

(14) (a) Garnweitner, G.; Smarsly, B.; Assink, R.; Ruland, W.; Bond, E.; Brinker, C. J. *J. Am. Chem. Soc.* **2003**, *125*, 5627. (b) Smarsly, B.; Garnweitner, G.; Assink, R.; Brinker, C. J. *Prog. Org. Coat.* **2003**, *47*, 393−400.

(15) Schild, H. G. *Prog. Polym. Sci.* **1992**, *17*, 163−249.

(16) Churochkina, N. A.; Starodoubtsev, S. G.; Khokhlov, A. R. *Polym. Gels Networks* **1998**, *6*, 205.

(17) Ruland, W.; Smarsly, B. *J. Appl. Crystallogr.* **2004**, *37*, 575−584.

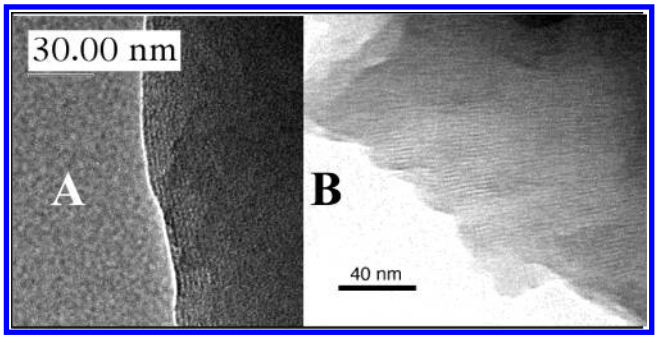

Figure 1. TEM micrographs of a lamellar mesostructured polymer/silica nanocomposite film after heat treatment (A) and after surfactant removal (B).

sonication and filtering, films were prepared on silicon substrates by dip-coating in dry N_2. Heat treatment (120 °C for 3 h in N_2) was employed to polymerize the monomers and condense the silica framework. Finally, the samples were washed successively in ethanol and acetone to remove the surfactant and any unreacted monomers.

SAXS experiments were carried out on a $\theta-\theta$ diffractometer, using a Siemens D500 instrument featuring Cu Kα radiation, filtered with Ni. The GISAXS experiments were performed at the Advanced Photon Source (APS) at Argonne National Laboratories on the 1-BM-C beamline. A 2D CCD detector (Bruker) was used to acquire the data, the pixel size being 0.16 × 0.16 mm. The wavelength was $\lambda = 0.112\,74$ nm (Si(111)) by the Physical Sciences Lab, and the sample–detector distance was 39 cm.

The thickness measurements were made with a J.A. Wollam Co. M44 spectroscopic ellipsometer using a Cauchy dispersion model to determine film optical constants. Refractive index profiles were assumed to be step-index, corresponding to a homogeneous film structure. The validity of the thickness measurements was tested by studying various points on one particular sample, taking the average for the data shown below. Transmission electron microscopy (TEM) was performed on a JEOL 2010, operating at an accelerating voltage of 200 kV and equipped with a Gatan slow scan CCD camera. TEM samples were prepared by scraping the film with a sharp blade and transferring the flakes to a carbon-coated copper grid. Imaging was performed in underfocus conditions.

TGA was performed on a TA Instruments Simultaneous Differential Techniques (SDT) 2960 device. The standard heating rate applied was 1 °C/min, starting at ambient temperature and ramping up to 600 °C. Typically, 10–20 mg of sample was used for the measurement.

The ^{13}C NMR spectra were recorded with ^{1}H decoupling on a Bruker DRX spectrometer at 100.6 MHz using a 5 mm broadband probe. The polymers were swollen in tetrahydrofuran-d_8 and heated to 60 °C during measurements. Typically 1024 scans were recorded with a 5 s delay between scans. The spectra were processed with 10 Hz exponential line broadening.

Results and Discussion

1. Transmission Electron Microscopy. Figure 1 shows TEM images of specimens obtained from films after heat treatment and after surfactant removal and washing in water. Parallel layers are observed, extending over micron-sized domains, showing a high perfection in terms of the layer thicknesses, as already previously described for similar systems.[10] It is difficult to obtain high-quality TEM images due to the significant content of organic matter. From the TEM images, one obtains a layer-to-layer distance of ca. 4 nm, which is in agreement with SAXS (see below). It is important to emphasize that TEM alone does not allow an unambiguous conclusion about the exact nature of such mesostructures (lamellar, 2D hexagonal, etc.); therefore these materials always have to be subjected to a detailed SAXS characterization.

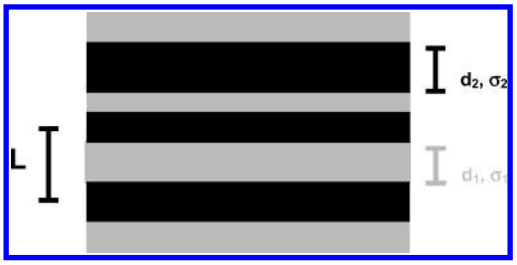

Figure 2. Illustration of a lamellar two-phase system showing the corresponding structural parameters of the SAXS analysis (see the text for the definition of the parameters).

2. Structural Characterization by SAXS. 2.1. SAXS Theory of Lamellar Two-Phase Systems. In the general theory of SAXS, a lamellar nanocomposite can be regarded as a lamellar two-phase system of two types of alternating layers of different, constant electron densities.[1] A lamellar two-phase system can be described by the long period L and the thicknesses d_1 and d_2 of the constituting lamellae (see Figure 2). In real systems, d_1 and d_2 are polydisperse and show variances σ_1 and σ_2. Thus, such a system can be regarded as a 1D point lattice, modulated by the size distributions for d_1 and d_2. Different scenarios can be envisaged for the statistics of d_1 and d_2, which were described by Ruland et al.[17,19] The following analysis represents an extension of this approach, which describes lamellar two-phase systems by the so-called "lattice model" and the "stacking model".[17] In the lattice model, the points of this lattice represent the centers of the lamellae of one kind, while the thickness statistics of this layer and the statistics of the 1D lattice are supposed to be independent. In the stacking model, which was used for the analysis, the thicknesses of the two layers show a statistically independent variation. So far, these models have mostly been used for microphase-separated block copolymers but were not applied to thin nanocomposite films. As will be demonstrated by GISAXS, the present lamellar mesostructures show a high degree of preferred orientation relative to the substrate, the SAXS of which is given by

$$I(\vec{s}) = \Phi_D{}^2(s_{12})I_1(s_3) \tag{1}$$

where $\vec{s} = (s_1,s_2,s_3)$ represents the scattering vector in a rectangular coordinate system with $|\vec{s}| = (2/\lambda)\sin(\theta)$ with $s_{12} = (s_1{}^2 + s_2{}^2)^{1/2}$; 2θ is the scattering angle. Φ_D represents the shape amplitude of the cross section of the lamellae, and I_1 (s_3) is the 1D SAXS intensity distribution of the stacks of lamellae. If the lateral extension of the lamellae is large compared to the periodicity of the lamellae, assuming a perfect alignment of the lamellae parallel to the substrate, one obtains

$$I(s_{12}, s_3) \propto \delta(s_{12})I_1(s_3) \tag{2}$$

For the stacking model with infinitely high stacks, we obtain

$$I_1(s) = \frac{1}{s^2}\mathrm{Re}\left[\frac{(1 - H_1(s))(1 - H_2(s))}{1 - H_1(s)H_2(s)}\right] \tag{3}$$

with

$$H_j(s) = \exp(2\pi i d_j s - 2\pi^2\sigma_j{}^2 s^2)$$

(18) Ruland, W. *Colloid Polym. Sci.* **1977**, *255*, 417.
(19) Wolff, T.; Burger, C.; Ruland, W. *Macromolecules* **1994**, *27*, 3301–3309.

where d_j are the thicknesses of the two types of constituting layers with their corresponding variances σ_j. In eq 3, it is assumed that the stack height is infinitely high: as already pointed out previously,[10,14] for not too thick films the average stack height corresponds to the entire film thickness, which is about 250−400 nm. The broadening of SAXS interferences due to the finite film height is negligible compared to the width induced by the variances σ_j and the finite instrumental resolution of our instrument, the latter being taken into account by a convolution of $I_1(s)$ with a Gaussian profile. A complete theoretical study on the SAXS of oriented lamellar nanocomposites is given in a separate publication,[17] addressing the separation of the effects of finite stack sizes and the influence of a finite instrumental resolution. Also, the theoretical influence of a finite preferred orientation on SAXS data is treated in detail. The present study has to be regarded as an application of the theoretical SAXS treatment given in ref 17; therefore the theoretical details are omitted here.

2.2. Additional Theoretical and Experimental Parameters Affecting the SAXS of Oriented Lamellae. While eqs 1−3 describe the theoretical SAXS measured with a point focus, the observed SAXS patterns $I_{exp}(s)$ can be influenced by further experimental and structural effects. The slit collimation of standard diffractometers leads to a smearing $I_{sm}(s)$ of SAXS patterns with

$$I_{sm}(s) = \int_0^\infty I_1(\sqrt{s^2 + y^2}) W(y)\, dy \qquad (4)$$

where $W(y)$ denotes the beam profile,[20] which was estimated from the diffractometer geometry (radius, slit size), and it was assumed that $W(y)$ has a rectangular shape. While we calculated SAXS curves based on eq 4, an approximation is demonstrated in ref 17. Also, the influence of absorption effects has to be taken into account by the absorption factor for symmetric reflection $A(\theta) \propto 1 - \exp[-2\mu t/\sin\theta]$, where t is the sample thickness and μ is the linear absorption coefficient. Based on the average densities of amorphous silica and the bulk polymers/surfactant, we assumed $\mu = 40\ cm^{-1}$. In addition, the influence of an interface of finite width d_z between the two layers constituting the lamellar structure was taken into account using the factor $H_z^2(s) = \exp(-2\pi d_z^2 s^2)$.[18] The final expression used for the fit of the experimental SAXS data is thus given by

$$I_{fit}(s) = kA(s)\{I_{sm}(s)H_z^2(s) + I_B(s)\} \qquad (5)$$

If necessary, the intensity distribution has to be smeared by the finite instrumental resolution and the slit geometry, but here an approximation was used according to ref 17. $I_B(s)$ represents a nonconstant background scattering from density fluctuations according to ref 18, of the form $I_B(s) = a + bs^2$ with parameters a and b. In conclusion, the fitting parameters are k, d_1, d_2, σ_1, σ_2, d_z, a, and b.

2.3. Testing of the Algorithm with Simulated Data. Since the analyses of SAXS data (section 2.4) are based on the determination of various parameters of a lamellar mesostructure, especially d_1 and d_2, it has to be assured that these parameters can be obtained from experimental data with sufficient accuracy, which may be blurred by statistical noise and background scattering. The validity of the evaluation approach was tested using simulated SAXS data of a lamellar two-phase system, which were

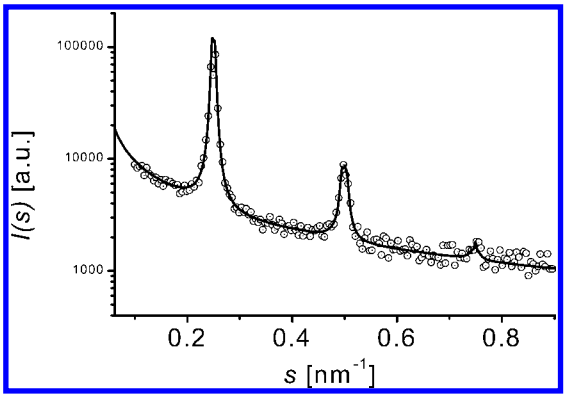

Figure 3. Simulated SAXS data (hollow circles) and fit based on the approach in section 2.1 (see Table 1).

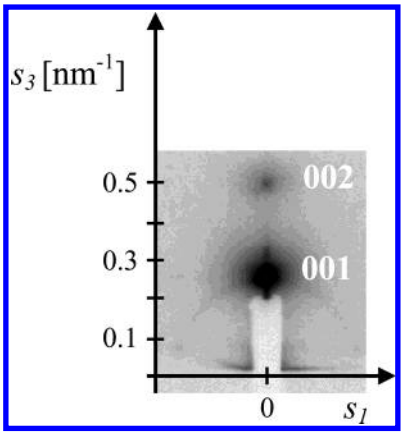

Figure 4. 2D GISAXS pattern of a nanocomposite film after heat treatment, containing PDM/PNIPAM polymers. The two equidistant reflections in the s_3 direction indicate the presence of lamellae oriented parallel to the surface.

Table 1. Comparison of Theoretical Values and Parameters Obtained from Fitting Simulated Data, Based on Equation 5

parameter	theoretical values	fitted values	parameter	theoretical values	fitted values
d_1 [nm]	1.0	0.99	d_z [nm]	0.65	0.58
σ_1 [nm]	0.08	0.04	a	0.4	0.35
d_2 [nm]	3.0	3.02	k	48000	53203
σ_2 [nm]	0.06	0.08			

then analyzed by our approach (eq 5), using a standard least-squares Gauss−Newton routine for nonlinear curve fitting. The simulated data were blurred artificially with statistical noise. An additive, constant background scattering was included, the amplitude of which being comparable to our SAXS experiments. Also, the values for the structural parameters were similar to those of the real films. The simulated data were cut off at small and large scattering vectors, comparable to our in-house X-ray instrument. The statistical noise was created by assuming Poisson statistics, as predicted by theory. It is seen (Figure 3) that our approach fits the simulated SAXS data excellently over almost the whole s range for the stacking model. More importantly, the parameters d_1 and d_2 obtained from the fitting procedure are in good agreement with the theoretical values, which was observed for several simulations. Also d_z, σ_1, and σ_2 can be at least obtained with a moderate accuracy (see Table 1). The data could also be fitted using the lattice model, providing almost identical parameters (not shown). In conclusion, it can be stated that our evaluation approach represents a suitable procedure to quantitatively analyze the SAXS of lamellar

(20) Smarsly, B.; Antonietti, M.; Wolff, T. *J. Chem. Phys.* **2002**, *116*, 2618.

Table 2. Structural Parameters for a Lamellar Mesostructure for Films of Different Compositions, Obtained from Fitting the Corresponding SAXS Data[a]

	composition/treatment	d_1 [nm]	d_2 [nm]	L [nm]	σ_1 [nm]	σ_2 [nm]	d_z [nm]
I	CTAB/SiO_2, as-prepared (Figure 5A)	1.07	2.83	3.90	0.13	0.13	0.5
II	CTAB/SiO_2, heat treated (Figure 5A)	0.92	2.72	3.64	0.16	0.11	0.5
III	CTAB/SiO_2, washed (−)						
IV	CTAB/7-OTS/SiO_2, as prepared (not shown)	0.90	2.67	3.57	0.07	0.12	0.65
V	CTAB/7-OTS/SiO_2, heat-treated (Figure 5B)	0.65	2.30	2.95	0.13	0.20	0.65
VI	CTAB/7-OTS/SiO_2, washed (−)			1.40			
VII	CTAB/7-OTS/PNIPAM/PDM/SiO_2, as-prepared (Figure 5A)	1.25	2.94	4.21	0.15	0.3	0.7
VIII	CTAB/7-OTS/PNIPAM/PDM/SiO_2, heat-treated (Figure 5B)	0.7	2.0	2.7	0.1	0.2	0.65
IX	CTAB/7-OTS/PNIPAM/PDM/SiO_2, washed, dried state (Figure 10, curve 1)	1.0	0.9	1.9	0.2	0.15	ca. 0.6−0.7
X	CTAB/PNIPAM/PDM/SiO_2, heat-treated (Figure 8A)	1.03	2.86	3.89	0.11	0.23	0.7
XI	CTAB/PNIPAM/PDM/ SiO_2, washed (Figure 8A)			(1.2)			

[a] The corresponding figures are indicated. (−) means that the mesostructure is destroyed.

nanocomposite films with respect to the major parameters determining oriented lamellar mesostructures, especially d_1 and d_2.

2.4. Quantitative SAXS Evaluation of Polymer–SiO_2 Nanocomposite Films. 2D GISAXS was used to verify that indeed lamellar mesostructures are created and to estimate the degree of preferred orientation. Figure 4 shows a 2D GISAXS pattern obtained from a film containing DM and NIPAM after the heat treatment step, containing DM and NIPAM. Two distinct reflections (d_{001} = 3.7 nm) are observed in the s_3-direction, thus unambiguously proving the presence of a lamellar mesostructure with the lamellae being parallel to the substrate. The narrow width of the reflections indicates a very high degree of preferred orientation.

To study the structure and composition of the nanocomposite films and to understand the details of the self-assembly in the presence of the monomers and the coupling agent (7-OTS), SAXS was performed on films of different compositions, using a standard $\theta-\theta$ diffractometer in symmetric reflection. The SAXS data were evaluated by the approach in eq 5, using the stacking model, providing a set of structural parameters for the lamellar mesostructures. As is evident from Figure 5, it is remarkable that all the SAXS profiles, showing different shapes, can be fitted excellently over the whole SAXS range. On one hand, this finding proves the applicability of the evaluation for materials with significantly different values for d_i and σ_i. On the other hand, this observation demonstrates the uniformity of the lamellar mesostructures, because the underlying structure model is relatively simple and contains only a limited number of parameters. The structural parameters are summarized in Table 2, also indicating the corresponding figure. Comparing the results with respect to the treatment and the composition, several interesting features were observed (see also ref 17):

(i) The layer thicknesses d_1 and d_2 are significantly different from each other for all samples, with d_1 being of the order of ca. 0.8−1.1 nm and d_2 = 2−3 nm, depending on the composition. Based on TGA (see Table 3), layers 1 and 2 are attributable to the silica and organic layer, respectively.

(ii) In general, the layer thicknesses d_1 and d_2 decrease during the heat treatment step due to the evaporation of solvent and the silica condensation.

(iii) For all the samples, the finite interface boundary has a significant value of d_z = 0.5−0.7 nm, which is almost of the order of d_1 (silica layer) itself. In conclusion, especially the silica layer cannot be regarded as a layer of constant density but shows a certain transition toward the organic layer. Interestingly, d_z seems to be slightly larger for samples containing 7-OTS, which might be attributable to the organic moiety located at the interface.

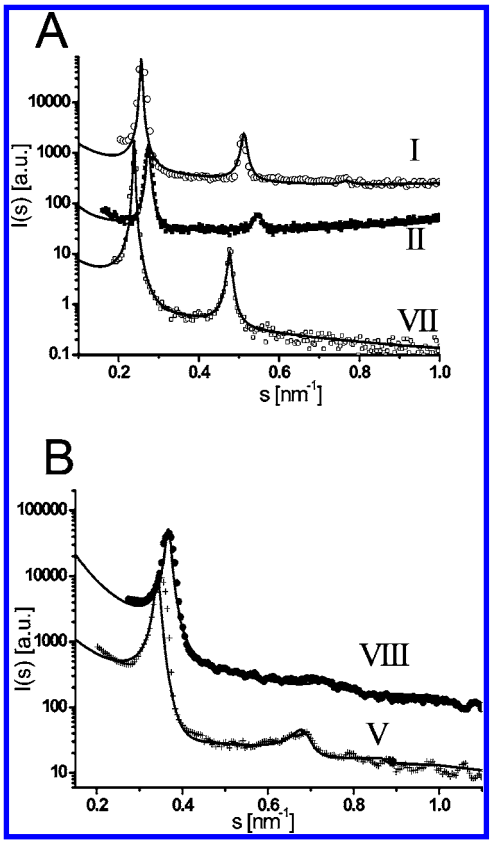

Figure 5. SAXS data and corresponding fits (solid lines). (A) Sample I (CTAB/SiO_2, as-prepared, hollow circles), sample II (CTAB/SiO_2, heat-treated, filled squares), and sample VII (CTAB/SiO_2/7-OTS/PNIPAM/PDM, as-prepared, hollow squares, see also ref 17). (B) Sample V (CTAB/SiO_2/7-OTS, crosses) and sample VIII (CTAB/SiO_2/7-OTS/PNIPAM/PDM, heat-treated, hollow squares, see ref 17).

(iv) The films prepared from solutions containing monomers (DM/NIPAM) possess a larger organic layer (sample VII) compared to a film consisting only of CTAB/SiO_2 (sample I), demonstrating that indeed the final polymer is located in the organic surfactant layer between the silica sheets.

(v) The incorporation of the monomers does not lead to a major distortion of the lamellar mesostructure, as is seen in the σ_i values of samples I/II (CTAB/SiO_2) and VII/VIII (CTAB/SiO_2/PNIPAM/PDM). It is seen that also the temperature treatment itself does not introduce significant disorder into these films.

(vi) After washing (surfactant removal), only the samples containing both 7-OTS and NIPAM/DM show a distinct SAXS pattern, the significant width of which

Table 3. Information Extracted from TGA Data[a]

	composition/treatment	content [wt %] CTAB	PNIPAM/PDM	SiO_2	7-OTS	$\phi(SiO_2)/\phi$(organics) (TGA)	d_1/d_2 (SAXS)
II	CTAB/SiO_2, heat-treated[b]	52		46		0.40	0.33
III	CTAB/SiO_2, washed (−)						
V	CTAB/7-OTS/SiO_2, heat-treated[b]	37		41	19	0.34	0.28
VI	CTAB/7-OTS/SiO_2, washed[b]	4		71	21	1.30	
VIII	CTAB/7-OTS/PNIPAM/PDM/ SiO_2, heat-treated[b]	28	35[d]	29	n.a.	0.37	0.35
IX	CTAB/7-OTS/PNIPAM/DM/ SiO_2, washed[b]		25[c,d]	75	n.a.	1.40	1.1
X	CTAB/PNIPAM/PDM/ SiO_2, heat-treated (Figure 8B)	34	20	44		0.37	0.37
XI	CTAB/PNIPAM/PDM/ SiO_2, washed (Figure 8B)		2				
XII	PDM/SiO_2, shortly heat-treated		29[e]	71		1.10	
XIII	CTAB/PDM/SiO_2, heat-treated	31	33	31		0.22	see ref 14b

[a] The theoretical values are put in brackets (based on the composition of the corresponding starting solutions). The content of the different species is compared with the volume ratio d_1/d_2 obtained from SAXS data (see Table 1). [b] See the Supporting Information. [c] Including the water content determined from TGA. [d] Including 7-OTS. [e] Including monomers.

probably being attributable to an inhomogeneous thickness of the polymer layers. Furthermore, since the GISAXS pattern still shows a high degree of orientation for the washed samples (see section 6/Figure 11), washing does not break down the lamellar mesostructure, if the polymers are covalently linked to the silica matrix.

(vii) A closer look at the thicknesses d_i reveals interesting relationships between the composition of the starting solution and the final lamellar mesostructure. For instance, sample VII (as-prepared after dip-coating, containing NIPAM/DM monomers) shows a larger value for d_2 (organic layer) than sample I due to the incorporation of monomers. However, after the heat treatment the d_2 value of sample II is larger than that of sample VIII, although sample VIII contains polymers in addition to CTAB. The TGA decay experiments revealed that the composition of sample VIII is in good agreement with the theoretical composition as calculated from the concentrations in the starting solutions (see the tables). A similar trend is observed for a comparison of sample V (7-OTS/CTAB/SiO_2) and sample VIII. First, one possible explanation is the loss of monomers through evaporation (up to 30%), as already reported in our previous publication, which is however not sufficient to account for this inconsistency. Second, it has to be considered that the presence of polymers and 7-OTS disturbs the packing of CTAB molecules, thus reducing the number of CTAB molecules per unit volume. This assumption is supported by a comparison of d_2 between sample V (7-OTS/CTAB/SiO_2) and sample II (CTAB/SiO_2). Third, we believe that this apparent uncertainty can be resolved by taking into account the different values of d_z determined for these samples: assuming that the "true" silica and organic layer thicknesses can be approximated by $d_i + 0.5d_z$, the organic layer thickness d_2 becomes comparable for these samples.

3. Analysis of Sample Composition by TGA. 3.1. General Aspects. TGA represents a straightforward and ideal tool for determining the composition of polymer/inorganic nanocomposites, because the remaining material at high temperature is clearly attributable to the oxide. Thus, all heat-treated and washed samples characterized by SAXS were also subjected to TGA analysis for a verification of d_1 and d_2 obtained from SAXS. A perfectly condensed SiO_2 matrix was assumed to be present after the heat treatment. In principle, the TGA curves of the present films are a complex superposition of the degradation/evaporation of CTAB, 7-OTS, silica, EtOH, water, and the polymers. The decomposition of CTAB was found at 180−280 °C; thus, the weight decrease in this range was attributed to the surfactant, whereas the polymers decomposed at higher temperatures (300−550 °C). The content of 7-OTS could not be calculated separately from the polymer content in mixed samples due to simultaneously occurring decomposition. For calculation of the volume ratio of silica to the organic material, the density of silica was estimated as 2.2 g cm^{-3}, whereas the polymer and surfactant density was assumed to be about 1.0 g cm^{-3}. The obtained data are shown in Table 3; they are in good consistency to the SAXS results even though the obtained volume ratios can only be taken as an estimate: the amount of sample obtained by dip-coating of silica films was too low for a reliable TGA measurement; therefore the material was prepared by casting the solution onto a Petri dish (except for sample IX), resulting in a substantially higher film thickness aggravating evaporation of the solvent and any condensation products upon heat treatment. Because of the larger film thickness, the washing procedure is expected to be less efficient compared to that for dip-coated films. This can be seen for sample VI: about 4% of the CTAB molecules are left even after thorough washing, whereas no CTAB was found for sample IX, which was the only sample prepared on a Si wafer. Samples III and XI became detached from the substrate upon washing, which is in accordance to observations made with the respective samples prepared for SAXS.

3.2. Decomposition Profiles. To compare the polymer content and the decomposition behavior of mesostructured films to that of nonordered films, TGA was performed using films prepared with and without surfactant. A silica−DM system was chosen to simplify analysis of the decomposition behavior (Figure 6A). The plots showing the derivative weight loss over temperature are illustrated in Figure 6B. Both samples were measured in the heat-treated state; however, for sample XIII, the treatment was combined with the TGA experiment by holding the temperature at 120 °C for 3 h before further heating, leading to a large weight loss at 120 °C due to evaporation of solvent. Sample XII was subjected to 120 °C for 1 h before measurement. As DM reacts rapidly, the degree of polymerization was high even after this shorter heat treatment; therefore, the two samples are still comparable. For the decomposition analysis, the derivative plots are more illustrative: for the nonstructured system, four maxima are found in the derivative plot. The signal at 125 °C is caused by evaporating monomer; the main decomposition was found at 248 and 465 °C and is clearly attributed to polymerized DM (PDM), as reported in the literature.[21,22] In comparison, a silica sample only showed

(21) Diez-Peña, E.; Quijada-Garrido, I.; Barrales-Rienda, J. M. *Polym. Bull.* **2002**, *48*, 83−91.
(22) Lazzari, M.; Kitayama, T.; Hatada, K.; Chiantore, O. *Macromolecules* **1998**, *31*, 8075−8082.

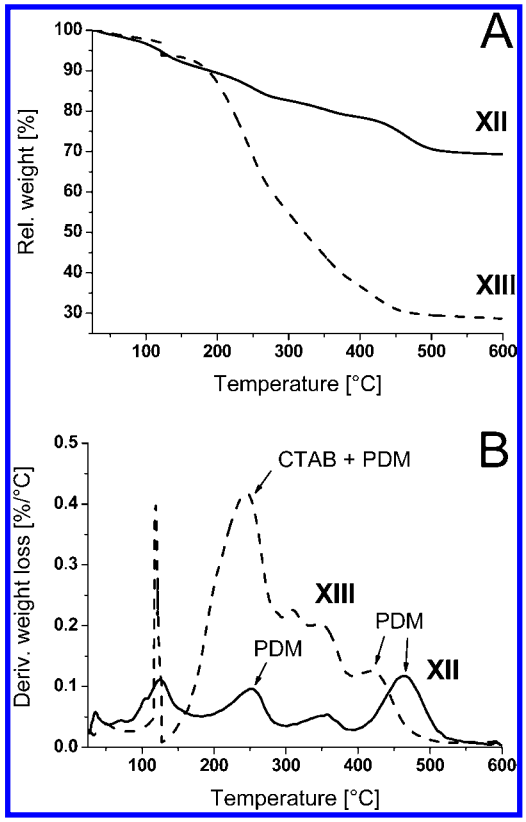

Figure 6. TGA data of a structured (sample XIII, containing a large amount of CTAB, dashed line) and a nonstructured (sample XII, containing no CTAB, solid line) silica–PDM system (after heat treatment, before washing): (A): weight loss over temperature; (B): derivative weight loss.

a slight, steady decrease in weight above 200 °C, amounting to no more than 6% in total. The mesostructured sample (sample XIII) shows a strong weight decrease around 240 °C, resembling mainly the decomposition of CTAB. Further signals are visible at 310 and 355 °C, which are attributable to PDM. The last decomposition step of the polymer occurs at 424 °C, which constitutes a significant shift compared to 465 °C for the nonstructured sample. This is interpreted as clear proof that the polymer is in a different chemical environment and cannot be situated within the silica matrix but is located in the "organic" layers. Also, it can be excluded that the polymer chains significantly penetrate the silica sheets.

4. Film Stability and Water Uptake Behavior. Since the characteristic swelling properties of hydrogels require a good access of water into the nanocomposite polymer layers, the films were studied by spectral ellipsometry, providing the overall film thickness *t* as a measure of the water uptake. In addition, these experiments allowed testing the film stability, which is known to decrease for SiO_2-based films upon treatment in water. In a recent study, it was demonstrated that the thickness of mesostructured silica films is a suitable measure for the film stability.[23] Figure 7 shows the film thickness obtained from various recipes, containing TEOS and CTAB (sample II); TEOS, 7-OTS, CTAB, and DM (sample X); and TEOS, 7-OTS, CTAB, DM, and NIPAM (sample VIII). The films were prepared by dip-coating (step 1), heat-treated at 120 °C (step 2), and washed in water (step 3). Afterward the films underwent repeated cycles of heat treatment at 60 °C (steps 4, 6, 8, and 10) and immersion in water (steps

(23) Dunphy, D. R.; Singer, S.; Cook, A. W.; Smarsly, B.; Doshi, D. A.; Brinker, C. J. *Langmuir* **2003**, *19*, 10403.

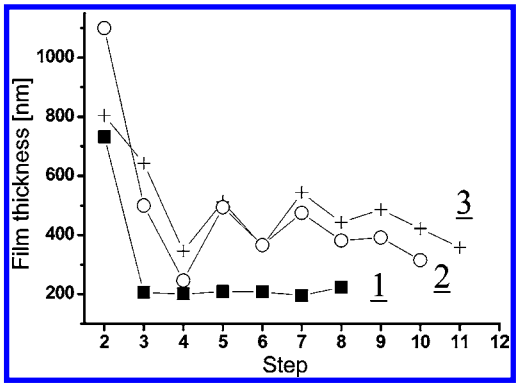

Figure 7. Film thickness as a function of the preparation steps and post-treatment by cycles of heating and immersing in water for films with different compositions of the solutions: (1) TEOS, CTAB; (2) TEOS, 7-OTS, CTAB, DM; (3) TEOS, 7-OTS, CTAB, DM, NIPAM. The points are connected for better visualization.

5, 7, 9, and 11), each step being monitored by ellipsometry. Step 1 is omitted in Figure 7, because it was difficult to study the samples under identical conditions after the dip-coating. The washing step clearly leads to a significant decrease in thickness as a consequence of the surfactant removal. Assuming that all of the surfactant is removed, the decrease in the film thickness for curve 1, acting as a reference, is in agreement with the CTAB content as determined from XRD. For sample I, the film thickness remained constant, probably only representing the thickness of the remaining SiO_2. For the samples containing hydrogels, the heating and water treatments resulted in a reversible shrinkage and increase in the thickness for several cycles by ca. 40%, which is attributable to the strong affinity of the hydrogels toward water. However, it turned out that the film stability is limited, as *t* remains constant at a low value after ca. 4 cycles, probably due to the general stability problems observed for silica-templated thin films. Recently, we have proposed that the addition of alumina species can improve the film stability toward water, which might be applicable also for the present nanocomposite films.[23]

5. Polymerization of NIPAM/DM/7-OTS. 5.1. Linkage of Polymers to the Silica Matrix. In our previous study, we had already reported that thermoresponsiveness was observed in films only if the solution contained all three double-bond-containing species DM, NIPAM, and 7-OTS, the details of which being unclear. Hence, films were prepared omitting the coupling agent 7-OTS and were studied by X-ray diffraction (XRD) and TGA. Figure 8A shows the SAXS data of such a film, after heat treatment and after washing, indicating that the heat-treated film possesses a well-defined mesostructure, while washing leads to an almost total structural collapse, thereby suggesting that the polymer is completely washed out. TGA analysis (Figure 8B) on the same films reveals a significant content of polymer after heating, while almost no polymer is left after washing. If compared to TGA data of a corresponding sample containing 7-OTS (sample IX), this observation proves that 7-OTS provides a strong linkage to the polymers, probably a covalent C–C bond. Interestingly, the preparation of thermoresponsive films failed without adding DM.[14] In particular, the films did not show any mesostructure after surfactant removal, thus indicating that PNIPAM did not react with 7-OTS and was not linked to the silica layers.[14] Thus, DM seems to mediate the linkage of PNIPAM to the siliceous matrix by forming a PDM–PNIPAM copolymer.

5.2. Copolymerization of DM and NIPAM. High-resolution solid-state ^{13}C NMR was used to study the

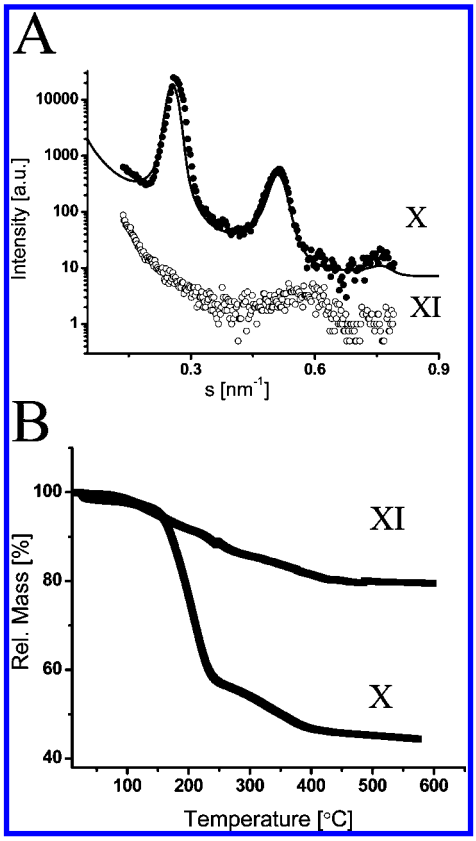

Figure 8. SAXS (A) and TGA data (B) of samples X and XI (sample prepared without adding 7-OTS, before and after washing).

formation of copolymers between DM and NIPAM (Figure 9). In general, the formation of statistical copolymers should lead to characteristic deviations in the signals of the CH_2 backbone, compared to the ^{13}C NMR spectra of the homopolymers.[24] The investigation of thin nanocomposite films was inappropriate, because the signals were inseparable from those of 7-OTS. Also, the low film sample quantities imposed further difficulties. Therefore, the NMR study was performed on bulk PDM (curve 1) and PNIPAM (curve 2) homopolymers and a polymer obtained from a solution containing a 1:1 ratio of DM/NIPAM (curve 3) that were swollen in THF at 60 °C. The well-resolved methyl resonances of the PDM are especially informative. The mr and rr stereoisomers resonate at 19.6 and 17.9 ppm,[24] respectively, in the spectrum of the homopolymer shown in Figure 9 (curve C1). Figure 9 (curve C2) demonstrates that the PNIPAM does not contribute to the ^{13}C spectrum in this region. The ^{13}C spectrum of the polymer prepared from the 1:1 mixture of NIPAM and DM is shown in Figure 9 (curve C3). Both stereoisomer resonances have significant shoulders, and an entirely new resonance appears at 18.9 ppm. The new peak indicates that some of the methyl group environments have been altered to a significant amount, consistent with at least one of the nearest neighbor DM units being replaced by a NIPAM unit. An analogous argument can be applied to the carbonyl resonances of PDM shown in Figure 9A. The carbonyl portion of the spectrum of PDM has several resonances that correspond to the various stereoisomers. The spectrum of PNIPAM shows that its carbonyl resonances are well separated from those of PDM. The carbonyl spectrum region of the polymer prepared

(24) Diez-Peña, E.; Quijada-Garrido, I.; Barrales-Rienda, J. M.; Wilhelm, M.; Spiess, H. W. *Macromol. Chem. Phys.* **2002**, *203*, 491.

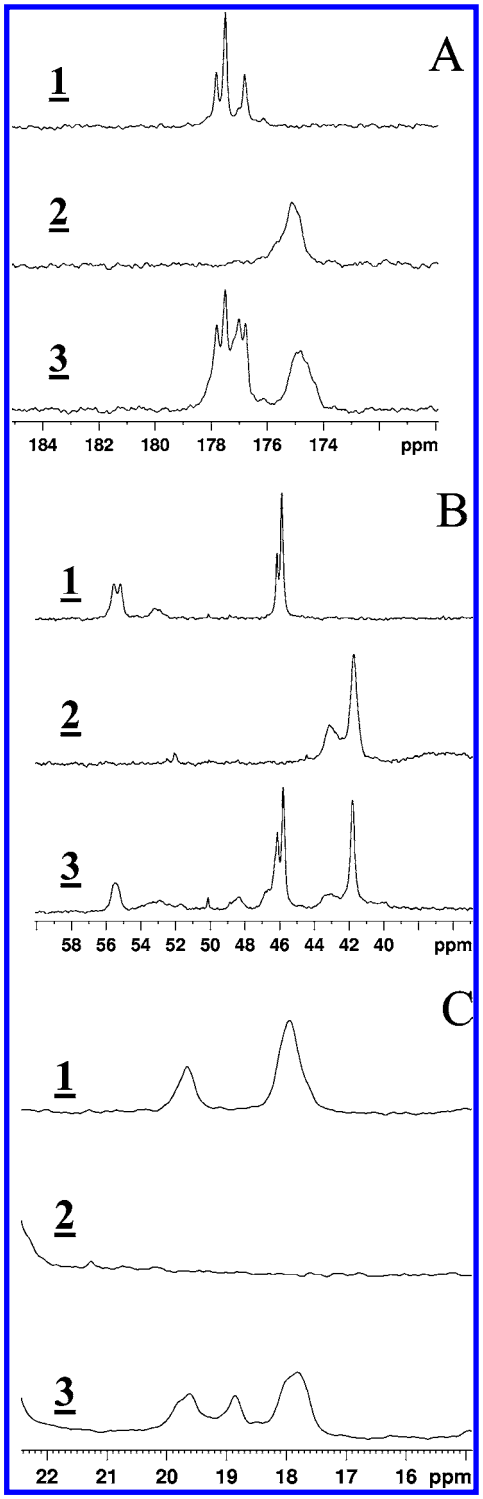

Figure 9. ^{13}C NMR studies of bulk polymers: (A) carbonyl region, (B) CH_2 backbone region, (C) aliphatic region; (1) pure PNIPAM, (2) PDM, (3) polymer prepared from a 1:1 mixture of NIPAM and DM.

from the 1:1 mixture again contains an additional resonance indicative of shifts caused by substitution at the nearest neighbor position. The resonances of carbons in the main chain of each of the polymers broaden or develop shoulders that are consistent with some random copolymerization of the 1:1 mixture. The isopropyl carbons in the PNIPAM are too distant from neighboring units to be affected.

The additional resonances in the methyl and carbonyl region show that the DM and NIPAM units do not

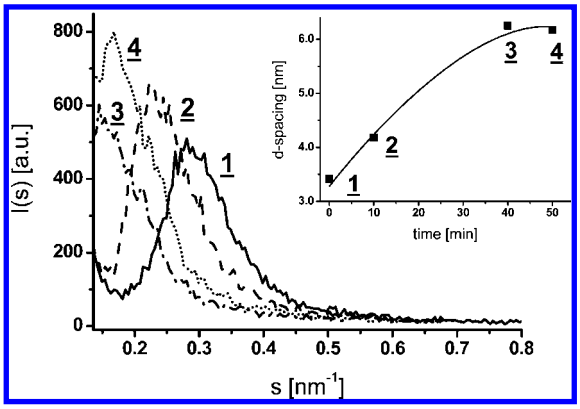

Figure 10. SAXS data for a PNIPAM/PDM–SiO_2 nanocomposite film, immersed in water, as a function of time. The film had been kept in water of $T = 50$ °C and was then immersed in water of $T = 25$ °C. SAXS scans were performed at equidistant time intervals of 10 min. The inset shows the increase in the *d* spacing as a function of time; the solid curve serves for better illustration.

polymerize in a block fashion. Since the resonances and shoulders cannot be completely assigned in terms of the various nearest neighbor possibilities, the exact degree of randomness cannot be calculated. The PDM methyl group resonances, which show the best resolution, suggest that a minimum of 30% of the DM units are adjacent to either one or two NIPAM units. As was pointed out recently,[24] the detection of statistical copolymerization between PNIPAM and methacrylates by NMR involves significant difficulties. Diez-Peña et al. used differential scanning calorimetry (DSC) to determine the lower critical solution temperature (LCST) as a function of the copolymer composition.[25] However, in our case the DSC signals turned out to be too broad for such analyses, thereby also supporting a statistical copolymerization (see the Supporting Information). In conclusion, the aforementioned experiments indicate that indeed a covalent linkage is formed between 7-OTS and the monomers. However, our findings suggest that this linkage can only be established through DM, but not through NIPAM. In addition, there appears to be a significant degree of random copolymerization between the DM and NIPAM units.

6. Swelling Behavior of NIPAM/DM Copolymer Films. While the successful swelling/deswelling of PNIPAM-containing nanocomposite films was already reported in our recent publication,[14] here we focus on suitable SAXS investigations addressing the reversibility and kinetics of this phase transition. For the time-dependent measurements using a diffractometer, a PNIPAM/DM nanocomposite film was kept in water of $T = 50$ °C for 6 h, then immersed in water of $T = 25$ °C for 10 min, and then placed into the XRD instrument for a scan of 2 min. Further analogous SAXS measurements were carried out by putting the sample into water of $T = 25$ °C for 10 min for several times. Although our instrument was not equipped with a temperature control, it is assumed that the sample temperature did not change much with the external temperature being $T = 24$ °C. The corresponding data are shown in Figure 10. A clear shift in the interference maxima to smaller scattering vectors is observed at lower temperatures, thus indicating a swelling of the polymer layers by ca. 2.5 nm, corresponding to an increase by a factor of 2. It is seen that the swelling amplitude reaches a plateau after ca. 30–40 min.

(25) Diez-Peña, E.; Quijada-Garrido, I.; Frutos, P.; Barrales-Rienda, J. M. *Macromolecules* **2002**, *35*, 2667.

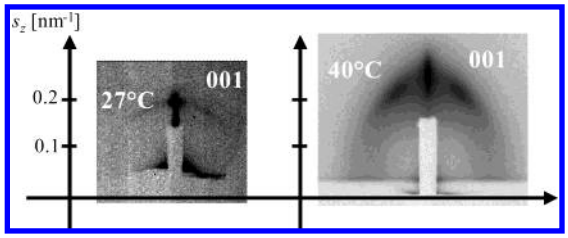

Figure 11. 2D GISAXS pattern of a lamellar nanocomposite film after washing, treated in water of $T = 27$ °C (left) and $T = 40$ °C (right). The temperature increase shifts the 001 reflection toward smaller scattering vectors.

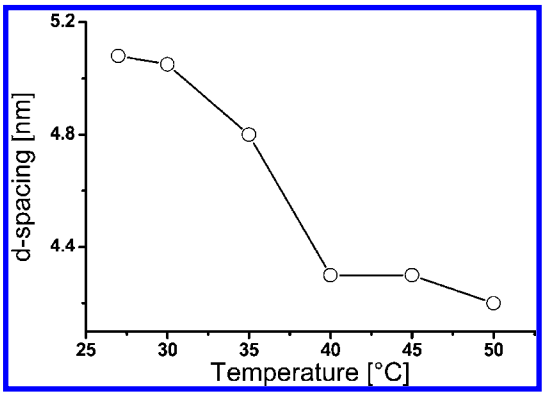

Figure 12. *d* spacing obtained from GISAXS as a function of the temperature for a lamellar nanocomposite PDM/PNIPAM–SiO_2 film. The points are connected for better visualization.

Since these SAXS experiments suffered from the lack of precise temperature control in the sample chamber, time-resolved measurements were carried out using the synchrotron facility at Argonne National Labs, Argonne, IL. A sample chamber with a heating stage was specially designed, also allowing control of the relative humidity around the films, while simultaneously performing diffraction experiments with a GISAXS setup. Also, this experiment was intended to determine the temperature of the PNIPAM phase transition. The swelling behavior was studied by immersing the film into water of $T = 25$ °C for 3 h and then placing it into the GISAXS sample chamber for 30 min with the relative humidity set to 50%; no significant change in the GISAXS was observed due to the evaporation of water. Unfortunately, the external temperature at the beamline was already about $T = 27$ °C, thus interfering with this temperature-sensitive experiment. The sample was then heated to 50 °C in steps of 5 °C with an equilibration time of 15 min. Figure 11 shows the GISAXS pattern of the sample at $T = T_0$ (27 °C) and $T = 40$ °C, indicating a decrease in the *d* spacing and the disappearance of the second-order reflection compared to the as-prepared film of Figure 4. The absence of a second-order reflection is in agreement with the XRD results shown above and reveals a loss in mesostructural order upon removal of the surfactant.

Nevertheless, the fact that the (001) reflection is preferentially oriented parallel to the s_3-axis indicates that the film still contains an oriented lamellar mesostructure. However, the (001) gets diffuse in the s_3-direction, which is in agreement with Figure 10. In Figure 12, the *d* spacing is plotted versus the chamber temperature, and a clear step is observed at about $T = 35$ °C, while the swelling amplitude is lower compared to Figure 10, probably partly due to the higher starting temperature of $T_0 = 27$ °C. Nevertheless, these in situ experiments enable us to conclude that the phase transition has a time scale on the order of 20–30 min and takes place at a temperature of

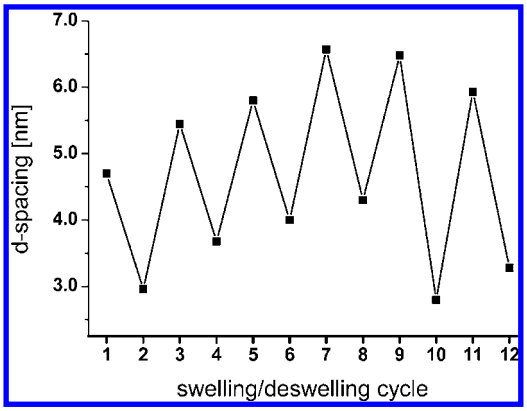

Figure 13. *d* spacing of a lamellar nanocomposite film, containing PNIPAM and PDM, immersed in water of $T = 5$ °C (uneven cycle numbers) and $T = 50$ °C (even cycle numbers). The points are connected for better visualization.

ca. 32 °C, which is in conformity with the LCST of PNIPAM. Also, the mesostructure remains preferentially oriented as revealed by the 2D GISAXS experiments.

To study the reversibility of the swelling/deswelling, a PNIPAM/PDM nanocomposite film was immersed in water of $T = 5$ °C and $T = 50$ °C for several times, each cycle monitored using an XRD diffractometer. It is clearly seen (Figure 13) that the expansion and contraction of the lamellae is fully reversible over a significant number of cycles. Interestingly, the magnitude of the phase transition seems to shift slightly, which might be due to the hindered uptake of water into the mesostructure.

Conclusions

The present study was intended as a thorough structural characterization of silica−hydrogel nanocomposite lamellar films. The SAXS approach presented showed to be an ideal method to depict fine structural details of the lamellar mesostructure on the angstrom scale. As a main result, it turned out that the incorporation of polymer (by adding an appropriate monomer to the sol−gel solution) does not lead to an accordingly large increase in the organic layer thickness (Figure 14). We attribute this finding to the evaporation of monomers but also to a principle limitation in the expansion of the organic layer: in essence, under the present conditions the organic phase cannot get larger than the inherent thickness of a surfactant bilayer. Therefore, the incorporation of polymer possibly results in lower surfactant content compared to films without polymer (Figure 14, sample IX), as confirmed by both SAXS and TGA. This interpretation is further supported by the finding that the addition of too much monomer distorts the mesostructure formation, because the surfactant is then insufficient to maintain the mesophase. This has to be regarded as a drawback of the present approach (route 4) to incorporate polymers into mesostructured materials. The study of the swelling behavior revealed a characteristic time scale for a complete phase transition of PNIPAM of ca. 30−60 min, which is larger than for pure PNIPAM systems, for example, PNIPAM microgels. This slow kinetics is probably a consequence of the low diffusion rate of water into the lamellar mesostructure. In this respect, these nanocomposite films will be not be suitable for fast-responding thermoresponsive devices. However, it is demonstrated that PNIPAM−silica hybrid films maintain the thermosensitivity of the pure polymer. In conclusion, the present study demonstrates that suitable SAXS methods have to be regarded as one of the few methods providing invaluable information on the composition and formation of polymer−inorganic materials. Thereby, the combination of SAXS with TGA represents a new methodology to study a wide variety of mesostructured polymer nanocomposites, in particular also composites of clays with polymers.

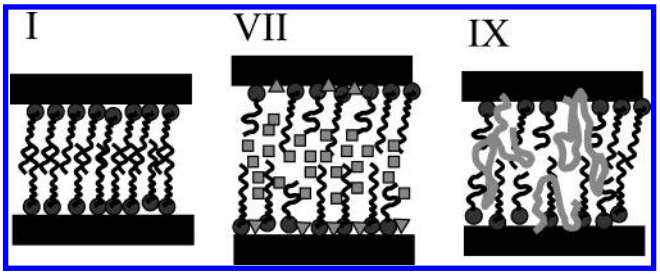

Figure 14. Sketch of the lamellar nanocomposite two-phase structure for various samples, illustrating the composition and the differences in the layer thickness: sample I (CTAB/SiO_2), sample VII (CTAB/SiO_2/7-OTS/PNIPAM/PDM, as-prepared), and sample IX (CTAB/SiO_2/7-OTS/PNIPAM/PDM, heat-treated). Squares, monomers; triangles, 7-OTS.

Acknowledgment. Sandia is a multiprogram laboratory operated by Sandia Corporation, a Lockheed Martin Company, for the United States Department of Energy's National Nuclear Security Administration under Contract DE-AC04-94AL85000.

Supporting Information Available: DSC curves of nanocomposite films with and without PNIPAM; thermogravimetric analysis. This material is available free of charge via the Internet at http://pubs.acs.org.

LA048962X